Large Eddy Simulation of a pistonless constant volume combustor: a new concept of pressure gain combustion

Nicola Detomaso*
CERFACS
42 avenue Gaspard Coriolis,
31057 Toulouse, France
Email: detomaso@cerfacs.fr

Davide Laera
CERFACS
42 avenue Gaspard Coriolis,
31057 Toulouse, France

Paul Pouech
CERFACS
42 avenue Gaspard Coriolis,
31057 Toulouse, France

Florent Duchaine
CERFACS
42 avenue Gaspard Coriolis,
31057 Toulouse, France

Thierry Poinsot
CERFACS
Institut de Mécanique des Fluides de Toulouse, IMFT
Université de Toulouse, CNRS, France

ABSTRACT

Classical gas turbine thermodynamic cycle has undergone no change over the last decades. The most important efficiency improvements have been obtained reducing thermal losses and raising the overall pressure ratio and peak temperature. Pressure Gain Combustion (PGC) represents an increasingly interesting solution to break out current technological limits. Indeed cycle models show that a pressure raise across the combustion process would reduce the fuel consumption, increasing the efficiency.

*Address all correspondence related to ASME style format and figures to this author.

Providing an efficiency close to the corresponding detonative technological concepts, Constant Volume Combustion (CVC) represents a viable solution that still needs to be studied. In the current work, the CV2 (Constant-Volume Combustion Vessel) installed at the Pprime laboratory (France) is numerically investigated using the high-fidelity compressible Large Eddy Simulation (LES) solver AVBP. All the successive phases of the CVC cycle, i.e. air intake, fuel injection, spark-ignited combustion and exhaust, are considered in the LES. Intake and exhaust valves are properly represented by novel boundary conditions able to mimic the valves impact on the flow without the need to directly consider their presence and dynamics during the simulation, reducing the computational costs. The spark ignition is modeled as an energy deposition term added to the energy equation. The combustion phase is treated by the dynamic version of the Thickened Flame model (DTFLES) extended to deal with non-constant pressure combustion. Time-resolved Particle Imaging Velocimetry (PIV) and pressure measurement inside the chamber reveal that cold and reactive turbulent flow are well captured in all the phases, showing the reliability of the approach and the models used.

NOMENCLATURE

Symbols

a ED model constant

A Section area

A_r Arrhenius pre-exponential factor

C_d Discharge coefficient

D_{st} Mass air-fuel ratio

E_a Arrhenius activation energy

f PEA correction function

k_f Forward reaction rate

L_{cyl} Cylindrical energy deposition length

m Mass

$\dot{m}$ Mass flow rate

M Mach number

M^w Molar mass

n_K Reaction exponent relative to the species k

P Static pressure

q Heat flux

$\dot{Q}$ Source term

R Mass-specific gas constant

R_d Spark radius

R_w Wall heat resistance

s_L^0 Laminar flame speed

T Static temperature

V Tank volume

Y_k Species mass fraction

Greek

β Turbulent combustion efficiency constant

γ Heat capacity ratio

δ_L^0 Laminar flame thickness

Δ_s Deposition size

Δ_t Deposition duration

Δp Pressure drops in the feeding tank

ϵ_d Deposited energy

ρ Static density

σ_s Deposition spatial parameter

σ_t Deposition temporal parameter

ϕ Equivalence ratio

Subscripts

1 First chemical reaction

2 Second chemical reaction

a Quantity evaluated for air

exh Quantity evaluated in the exhaust line

$exit$ Quantity evaluated in the outlet section of a generic De Laval nozzle

f Quantity evaluated for fuel

in Quantity evaluated in the LES inlet section

max Maximum value of a certain quantity

out Quantity evaluated in the LES outlet section

ref Reference value

t Quantity evaluated in the throat section

v Quantity evaluated in the valve section

$wall$ Quantity evaluated at wall cells

Superscripts

$*$ Quantity considered at the sonic condition

0 Quantity considered at stagnation condition

LES Quantity evaluated in LES

n Iteration at which a certain quantity is computed

sup Relative to a supersonic condition

sub Relative to a subsonic condition

INTRODUCTION

The European Climate Foundation [1] traced the path to reach the goal of a low-carbon Europe, investigating the technical and economic feasibility of achieving an 80% reduction in greenhouse gas emissions below 1990 levels by 2050, while maintaining or improving electricity supply reliability, energy security and economic growth. The thermodynamic cycle used in a gas turbine has undergone little changes since its early development. Over the last decades, effort has been put into increasing efficiency through reducing losses and raising overall pressure ratio and peak temperature. However, current concepts reached a plateau in terms of efficiency [2] and a techno-

logical breakthrough is needed to comply with these environmental constraints. One of the most promising is the Pressure Gain Combustion technology (PGC) where a pressure raise across the combustion process is allowed. Heiser and Pratt [3] highlighted, indeed, the beneficial impact of a lower entropy increase on the cycle efficiency. Theoretical cycle models show that an increase in total pressure around 15% - 20% can reduce aircraft fuel consumption from 4% - 9% also in modern turbofan [4]. Several PGC concepts are currently studied by the combustion community, ranging from deflagration to detonation [5]. Rotating Detonation Engine [4, 6, 7] and Pulse Detonation Engine [8, 9] utilize propagating detonation waves to increase pressure and temperature, raising significant engineering challenges [10].

Constant Volume Combustion (CVC) represents a viable solution to avoid this technical issues. According to [5], the thermodynamic efficiency, obtained using a constant volume combustion, is very close to that offered by detonation and can double the Brayton cycle gain. Hutchins and Metghalchi [11] compared the efficiency of the Brayton and the Humphrey cycles, taking the same heat of reaction, the same initial compression ratio, and isentropic expansion of the combustion products. A theoretical gain about 20% - 35% was found, justifying the interest in this new concept. Bobusch *et al.* [10] proposed a new way to implement CVC in a gas turbine combustion system using shockless explosion combustion. In this combustion concept, acoustic waves are used to fill and purge the combustion tube while the ignition is controlled by the auto-ignition delay time of the fuel-air mixture. An homogeneous auto-ignition can be generated working on this timing and no shock waves occur. The same model has been experimentally investigated by Yucel *et al.* [12] where the ignition distribution inside a stratified fuel–air mixture was analyzed.

Inspired by internal combustion engines, pistonless constant volume combustion combustors have represented another growing scientific field in the last years. Safran Aircraft Engines proposed a solution where the volume of the combustion chamber was opened and closed by rotating spheres. A similar concept has been studied experimentally by Boust *et al.* [13] and numerically by Labarrere *et al.* [14]. This rotating valves chamber, installed at the Pprime Institute (Poitiers, France), was created to prove the feasibility of the isochoric combustion at high frequencies, required for propulsion. The chamber was tested for a wide range of frequencies and a limit oper-

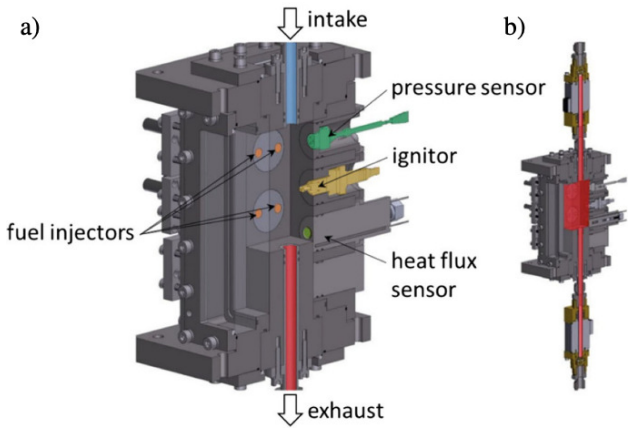

Fig. 1. CV2 configuration [15, 16]: a) combustion chamber key elements; b) the entire constant volume highlighted in red.

ating frequency was observed: after $40\ Hz$ the combustion speed was not enough to guarantee a complete combustion phase, intensifying cycle-to-cycle variations.

A novel CVC model called CV2 (Constant-Volume Combustion Vessel) was experimentally studied by Michalski *et al.* [15, 17, 18, 19] at the Pprime Institute. They focused on CVC stability considering different spark timing and different exhaust pressure to control the residual burnt gas levels. In high dilution cases some cycles experienced slow combustion which promoted an higher residual temperature leading to auto-ignition events in the next cycle. Although the literature addressing internal flows, ignition process and combustion phase in piston engines is sufficiently exhaustive [20, 21, 22, 23, 24, 25, 26, 27], it cannot be completely taken to CVC. Without a moving piston, intake turbulence is not dissipated leading to a scenario where the flame kernel, extremely sensitive to turbulence intensity, may be quenched. Computational Fluid Dynamics (CFD) can help the investigation of these phenomena swiping among the different combustors operating conditions. Large Eddy Simulation (LES) is an attractive and now widely used method to describe turbulent combustion including unsteady fluid phenomena like transient ignition [28], combustion instabilities [29] or cycle-to-cycle variations [14, 17, 24, 25, 30].

In the recent years LES has been used to tackle constant volume combustion and investigate the main fundamental problems that characterize it. Michalski *et al.* [16, 17] used LES to support experimental results [16, 18, 19] and investigate aspects which could not be evaluated during the experimental campaign. Labarrere *et al.* [14] studied numerically the isochoric combustion at

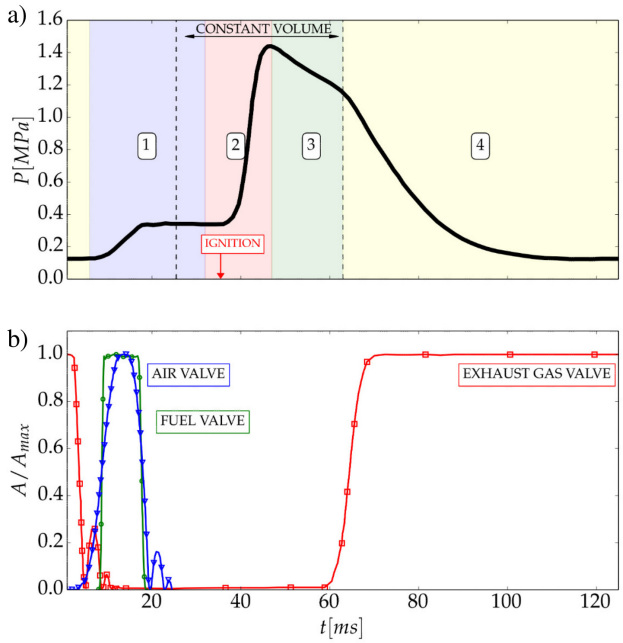

Fig. 2. (a) Pressure signal of the first reactive cycle with the different CV2 phases: admission and mixing 1, combustion 2, isochoric expansion 3, exhaust 4. At $t = 32.5\ ms$ ignition occurs. (b) Air (∇), fuel ($\circ$) and exhaust gas ($\square$) valve laws over the cycles [16, 19].

high frequencies computing the test bench installed at the Pprime institute during the experimental study of Boust *et al.* [13] showing how the flame kernel behaves on the turbulence intensity encountered, leading to a complete or incomplete combustion phase.

In the present work, the experiments performed in the CV2 test bench is investigated using the high-fidelity compressible LES solvers AVBP. Differently from previous studies [14] where the admission and exhaust phases of the CVC cycles have been simulated using moving meshes, novel boundary conditions able to properly mimic valves behavior are proposed in this work leading to a non negligible reduction of the complexity and the computational cost of the simulation. To compute the combustion phase, a novel global 2-steps chemical mechanism for propane-air combustion optimized for high pressure conditions is proposed and validated against detailed mechanism. A cylindrical energy deposition (Energy Deposition model) is used to represent the spark ignition while flame propagation is handled by an extended version of the dynamic thickened flame model (DTFLES [31]) able to correctly resolve the flame in non-homogeneous mixtures taking into account the variation of laminar flame thickness and speed with variable temperature and

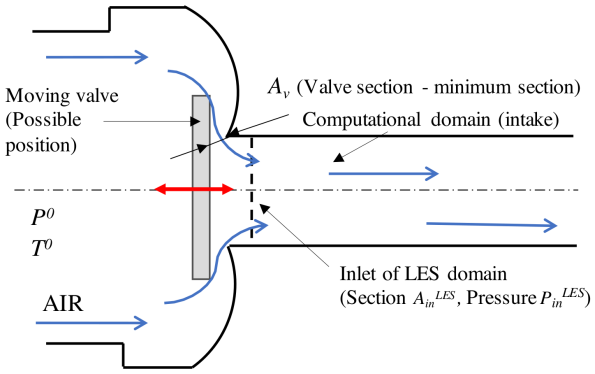

Fig. 3. Possible sketched position of the air inlet valve. Blue arrows indicate the flow streamlines and the dashed line indicates the computational inlet. The computational domain starts after the valve. Tank stagnation conditions: $P^0 = 10\,bar, T^0 = 300\,K$.

pressure.

The article is organized as follows: experimental set up and operating conditions are discussed in section 1. Then numerical model is described in section 2. The strategy adopted to write the boundary conditions is explained as well as the numerical modeling used to simulate ignition and combustion. In the last section, LES results for each phase of the CVC cycle are presented and discussed.

1 EXPERIMENTAL SETUP

The CV2 rig operated at Pprime laboratory (Poitiers) is representative of pistonless constant volume combustion configuration, relevant for air-breathing gas turbines. The chamber works cyclically and each cycle consists in three phases: air intake and fuel injection, ignition and combustion, exhaust. The combustion chamber is a squared high-strength stainless steel vessel (50 x 50 x 100 mm). Intake and exhaust sections are connected with the central volume by cylindrical tubes of inner diameter 12 mm, so that the overall chamber volume is 0.321 L (Fig. 1), as confirmed by water volume measurements.

The rapid intake is guaranteed by a single high-speed solenoid valve (COAX MK10) fed by a 20.76 L (0.3% uncertainty) tank, controlled in terms of both stagnation pressure (1.0 MPa) and fresh-air temperature. A 4.02 L (2.2% uncertainty) tank of gaseous propane (0.60 MPa, purity 99.95%) feeds four injectors (Fig. 1 (a)) which let the fuel enter directly the chamber. Ignition is obtained using an electric discharge supplied from a spark plug and an inductive ignitor (electrical

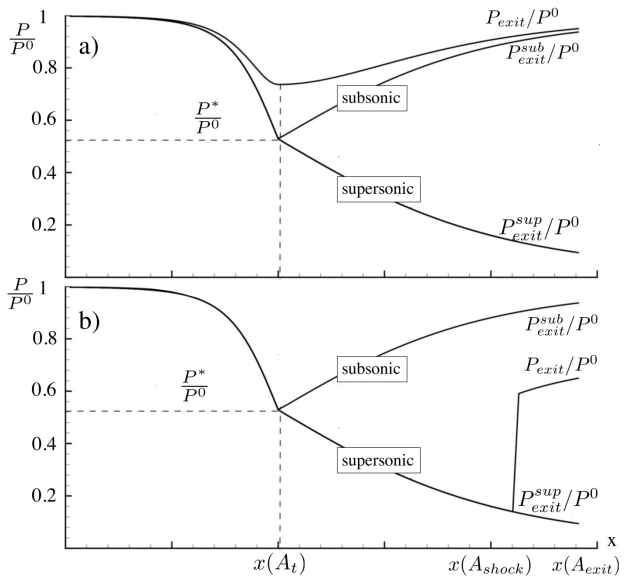

Fig. 4. Pressure evolution in a De Laval nozzle. P^{sub}_{exit} and P^{sup}_{exit} are the subsonic and supersonic solution of eqn. 4 evaluated on the generic De Laval exit section A_{exit}. a) Scenario with $P_{exit} > P^{sub}_{exit}$. b) Scenario with $P^{sup}_{exit} < P_{exit} < P^{sub}_{exit}$.

energy 40 ± 10 mJ). A second high-speed valve lets the burnt gases leave the chamber. A pressure-regulated tank controls the exhaust conditions. The valves section laws in time (Fig. 2 (b)) show that fuel is injected during the air intake phase and mixes with air until ignition occurs. The combustion chamber initially contains air at room temperature and at 0.1 MPa. The injected masses of fuel and air lead to an Overall Equivalence Ratio (OER) near unity.

A piezoresistive temperature-regulated sensor (Kistler 4049B) measures the combustion chamber pressure while an eroding junction surface thermocouple (Nanmac) provides wall heat flux measurements. Flame propagation is visualized by broadband chemiluminescence (visible wavelength) using a high-speed camera (Phantom v310, 12-bit). The high-speed PIV is based on a 20 KHz system (Nd:YAG MESA laser at 532 nm, and SA-Z Photron camera) and is used to characterize the velocity field: the final spatial resolution of the velocity field is 0.65 mm x 0.65 mm.

Twelve consecutive cycles have been experimentally characterized by Michalski *et al.* [15, 16, 17, 18, 19]. The pressure reached before combustion is 0.335 ± 0.007 MPa and the exhaust pressure was set to 1.0 bar. During all the cycles, the stagnation pressure in the admission tank undergoes a pressure drop of 4 % while the exhaust tank pressure increases of 40 %. These variations are even smaller in the propane tank. Experimentally, the OER is defined for each cycle

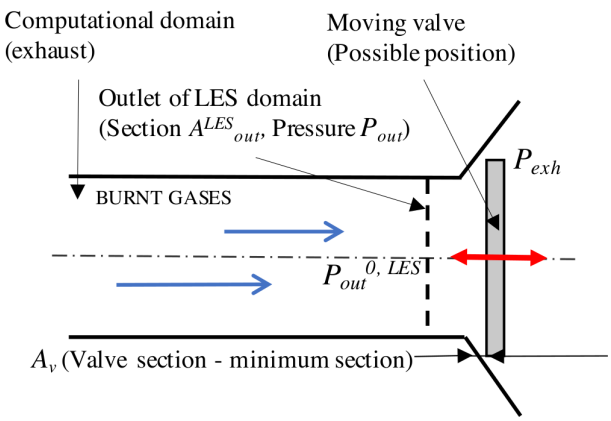

Fig. 5. Outlet valve sketch. The dashed line indicates the computational outlet. Blue arrows indicate the flow streamlines. The computational domain ends before the valve. $P_{out}^{0,LES}$ is the total pressure computed on the outlet section.

using the amount of mass of fresh air and of fuel injected in the chamber (Eqn. 1),

$$OER = D_{st}\frac{\gamma_a M_f^w \Delta p_f V_f}{\gamma_f M_a^w \Delta p_a V_a} \tag{1}$$

where M^W, Δp, V and γ are respectively the molar mass, pressure drops, the volume in the tanks and the heat capacity ratio of air and fuel while D_{st} is the mass air-fuel ratio of a stoichiometric propane-air mixture.

For the studied operative conditions, experiments show a 100% ignition success rate with a very limited cycle-to-cycle variations phenomena mainly due to the different dilution levels [15, 16, 17, 18, 19]. Figure 2 (a) shows the pressure signal of the first reactive cycle and clarifies the phases composing it. During the admission phase the air enters the chamber following a valve law that lasts 25.5 ms. Once the propane is injected through four annular nozzle (Fig. 1 (a)), it starts mixing with the fresh air in the closed volume. Ignition occurs at $t = 32.5$ ms and, during the flame propagation, temperature growth lets the pressure go up. At the end of the combustion phase, the temperature inside the chamber has reached its maximum value and it starts reducing thanks to thermal losses. Thus, a quick isochoric cooling, that lasts around 10 ms, anticipates the last phase, when the burnt gases flow in the exhaust tank. The valves section laws in time (Fig. 2 (b)) show an overlapping between the exhaust and the admission phase: part of the intake fresh air

is used to push the burnt gases out of the chamber, cleaning the volume. For both intake and discharge, while the admission and exhaust sections are reducing, the valves bounce against the seat until they are fully closed.

2 LARGE EDDY SIMULATION

The first reactive cycle (Fig. 2 (a)) is simulated using *AVBP* (http://www.cerfacs.fr/avbp7x/). The final conditions of the previous cycle ($P^0 = 1$ bar and $T^0 = 276$ K in the chamber) [16] are used as initial solution. The Navier-Stokes equations convective terms for reacting flows are solved with the TTGC scheme (3nd order accurate in space and time) based on a Taylor-Galerkin Finite Element approximation [32] and the diffusive terms are discretized applying the Galerkin finite element method to viscous fluxes [33]. The integration in time is explicit, limited by the acoustic CFL number (0.7). The subgrid Reynolds stresses are modeled by the WALE turbulent closure [34]. Walls are treated as no-slip and the inlet and outlet boundary conditions (BCs) are changed during the simulation to chain the cycle phases. Thermal losses are applied to the walls imposing a heat resistance compatible with the CV2 material ($R_w = 10^{-3}$ mK/W). Following this approach, the wall normal heat flux at iteration (n+1) is defined as:

$$q^{n+1} = -(T^n_{wall} - T_{ref})/R_w \tag{2}$$

where T^n_{wall} and T_{ref} are the temperature values computed at the wall cells and outside the chamber ($T_{ref} = T_w \sim 307$ [15]) respectively. With the value of R_w used, the boundary condition behaves like an isothermal no-slip wall.

A uniform mesh is used with a $\Delta x = 0.4$ mm while the spark ignition region is refined ($\Delta x = 0.1$ mm) to have a sufficient number of points in the energy deposition zone. Approximately 35 milion cells are used to discretize the whole domain.

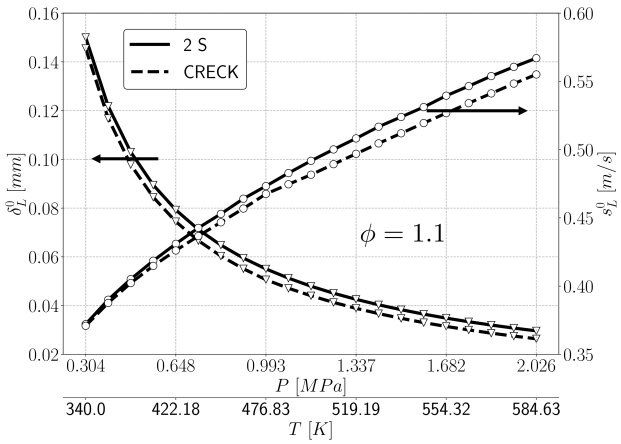

Fig. 6. Laminar flame speed (○) and laminar flame thickness (▽) of a 1D unstrained flame: 2 steps mechanism (solid lines) compared witht the detailed mechanism (dashed lines) [35].

Inlets and outlet boundary conditions for intake and exhaust phases

Valves are not included in the computational domain and they are substituted by novel boundary conditions based on the NSCBC formalism [36]. Figure 3 shows a sketch of the air intake valve: following the section law (Fig. 2 (b)), the air streamlines flow in the convergent part, reach the maximum velocity in the valve section (the minimum section) and then pass through a divergent part. A similar scenario happens for the fuel lines. Inlets boundary conditions are modelled assuming that the valves behave like a De Laval nozzle. A generic flow that undergoes an isentropic acceleration (if subsonic) or deceleration (if supersonic) up to sonic conditions, reaches a thermodynamic state described by its critical conditions (P^*, T^*, ρ^*). These quantities are function of the corresponding stagnation values and flow thermodynamic properties (Eqn. 3). For critical pressure, this writes as:

$$P^* = P^0 \left(\frac{2}{\gamma + 1} \right)^{\frac{\gamma}{\gamma - 1}} . \tag{3}$$

Recalling the De Laval correlations, if the flow becomes sonic in the throat section A_t ($A_t = A^*$, $P_t = P^*$, $T_t = T^*$, $\rho_t = \rho^*$) only two possible isentropic evolutions are allowed in the divergent

section: a subsonic and a supersonic one. These two solutions are sketched in Fig. 4 reporting the classical pressure evolution in a 1D De Laval nozzle [37]. Making use of the law relating the pressure, P, in a certain section A with the ratio between that section and A^* [37]:

$$\frac{A}{A^*} = \left\{ \frac{\gamma-1}{2} \left[\frac{2}{\gamma+1} \right]^{\frac{\gamma+1}{\gamma-1}} \left[\left(\frac{P}{P^0} \right)^{\frac{2}{\gamma}} - \left(\frac{P}{P^0} \right)^{\frac{\gamma+1}{\gamma}} \right]^{-1} \right\}^{\frac{1}{2}} \tag{4}$$

the two outlet pressure values P_{exit}^{sub} and P_{exit}^{sup}, corresponding, respectively, to the subsonic and supersonic solution relative to the section $A = A_{exit}$, could be computed. In particular, P_{exit}^{sub} corresponds to the highest possible pressure that can be reached in A_{exit}, given sonic throat condition and subsonic flow in the divergent. If the nozzle outlet pressure P_{exit} is between these two values, the throat section remains choked and a shock, in the divergent, adapts the pressure to the target. Finally, if P_{exit} is greater than P_{exit}^{sub}, the throat section is not choked anymore ($A_t \neq A^*$). In the proposed inlet boundary condition, the A_{exit} of the De Laval nozzle coincides with the inlet section of the LES computational domain, A_{in}^{LES}, while the valve section A_v is assumed to be the throat section (Fig. 3). Using these two area values in Eqn. (4) and knowing the tank stagnation pressure P^0, the two pressure values P_{in}^{sup} and P_{in}^{sub} at the LES inlet section can be computed. It is important to notice that, differently from a classical De Laval nozzle, these two values change in time because A_v is changing. Furthermore, the static pressure on the LES domain inlet section, P_{in}^{LES}, which is an output of the simulations, also varies in time during the intake phase. As a consequence, the flow behavior in the divergent part of the nozzle, which depends on the ratio between P_{in}^{LES} and P^0 also varies while the valve is opening. From previous discussion, multiple scenarios are possible to compute the target mass flow rate ($\dot{m}_{in}$) and the temperature (T_{in}) that should be imposed at the inlet BC according to the NSCBC theory to mimic this behavior[1]:

1. If $P_{in}^{sup} < P_{in}^{LES} \leq P_{in}^{sub}$ (Fig. 4 (b)), the valve section passage is choked ($A_v = A^*$, $P_v = P^*$). The target values of $\dot{m}_{in}$ and T_{in} can be computed as:

[1] Species mass fractions ($Y_{k,in}$) are also provided but flow composition is known a-priori.

$$\begin{cases} \dot{m}_{in} = C_d A^* \frac{P^0}{\sqrt{RT^0}} \sqrt{\gamma \left(\frac{2}{\gamma+1}\right)^{\frac{\gamma+1}{\gamma-1}}} \\ T_{in} = \frac{T^0}{\sqrt{1+\frac{\gamma-1}{2}(M_{in})^2}} \end{cases} \tag{5}$$

where the M_{in} is the Mach number on the LES inlet section, obtained applying the mass conservation law between the inlet section and the valve section.

2. If $P_{in}^{LES} > P_{in}^{sub}$ (Fig. 4 (a)) the solution in the De Laval nozzle is isentropic but the valve section is not choked ($A_v \neq A^*$, $P_v \neq P^*$). Mass flow and temperature can be derived as follows:

$$\begin{cases} \dot{m}_{in} = C_d A_{in} \frac{P^0\sqrt{\gamma}}{\sqrt{RT^0}} M_{in} \left[1 + \frac{\gamma-1}{2}(M_{in})^2\right]^{-\frac{\gamma+1}{2(\gamma-1)}} \\ T_{in} = \frac{T^0}{\sqrt{1+\frac{\gamma-1}{2}(M_{in})^2}} \end{cases} \tag{6}$$

where

$$M_{in} = \sqrt{\frac{2}{\gamma-1}\left(\left(\frac{P^0}{P_{in}^{LES}}\right)^{\frac{\gamma-1}{\gamma}} - 1\right)}. \tag{7}$$

R is the mass-specific gas constant and C_d is a discharge coefficient tuned in order to obtain the correct mass inside the chamber ($C_d^a = 0.67$, $C_d^f = 0.26$).

3. If $P_{in}^{LES} \leq P_{in}^{sup}$ a supersonic condition should be imposed at the LES inlet BCs. Nevertheless, for the specific application of the CV2, analysis on experimental mass flow rates show that the inlet section is always subsonic and an higher $\dot{m}$ would be necessary to reach supersonic condition in A_{in}^{LES}.

Therefore, conditions 1 and 2 are the only physically possible for the proposed BC which

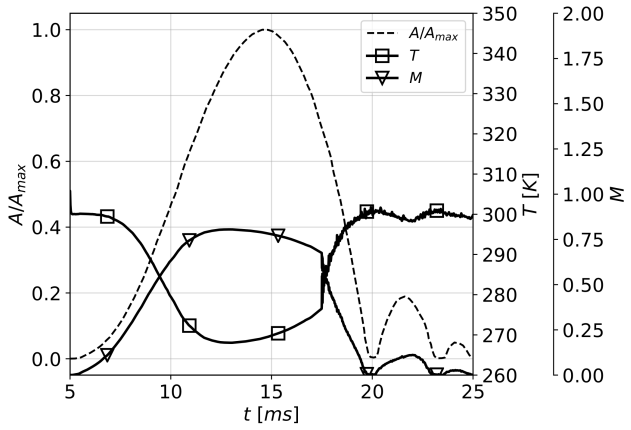

Fig. 7. Section law, temperature and Mach number evaluated on the inlet BC (air inlet).

requires as inputs the time evolution of the valve section area and the stagnation condition in the tank (assumed to remain constant for both air and fuel inlets).

For the exhaust phase, static pressure is imposed at the outlet LES section (A_{out}^{LES}) following the NSCBC formalism. Contrary from inlets, to evaluate the correct pressure target value P_{out} to be imposed at the BC, the outlet valve is assumed to behave like a simple convergent: the nozzle inlet section coincides with the outlet section of the LES computational domain, A_{out}^{LES}, and the minimum section is assumed to be the outlet valve section A_v (Fig. 5). The total pressure $P_{out}^{0,LES}$, which is computed on the LES outlet patch, reduces in time, whereas the exit pressure imposed downstream the valve exit remains constant and it is assumed equal to the experimental exhaust pressure $P_{exh} = 1$ bar. Also in this case, the critical sonic condition in the minimum section of the nozzle are given following the Eqn. (3) and the ratio between P_{exh} and $P_{out}^{0,LES}$ controls the flow behavior. Two scenarios are possible:

1. If $P_{exh}/P_{out}^{0,LES} \leq P^*/P_{out}^{0,LES} = \left(\frac{2}{\gamma+1}\right)^{\frac{\gamma}{\gamma-1}}$, the valve is choked ($A_v = A^*$,$P_v = P^*$). The target pressure P_{out} can be retrieved as the subsonic solution of Eqn. (4) by imposing $A = A_{out}^{LES}$.
2. If $P_{exh}/P_{out}^{0,LES} > P^*/P_{out}^{0,LES} = \left(\frac{2}{\gamma+1}\right)^{\frac{\gamma}{\gamma-1}}$, the valve is not choked ($A_v \neq A^*$, $P_v \neq P^*$), the flow can expand directly up to P_{exh} and P_{out} is obtained by applying the mass conservation law between the A_{out}^{LES} and A_v.

Differently from the inlet, the only input of the BC is the valve area law since the stagnation pressure on the outlet patch is retrieved by the simulation.

Ignition and turbulent combustion modelling

Chemistry, combustion and spark ignition are modeled in internal combustion engine and CVC, relying on the dynamic thickened flame model (DTFLES) [31] and the Energy Deposition (ED) model used in literature [14, 21, 24, 25, 30, 38, 39]. C_3H_8 - air flame chemistry is described using a novel 2-steps scheme based on Arrhenius type reaction rates. The first reaction of the scheme controls the laminar flame speed while the second one, $CO - CO_2$ equilibrium, guarantees the adiabatic flame temperature.

$$C_3H_8 + 3.5O_2 \rightarrow 3CO + 4H_2O \tag{8}$$

$$CO + 0.5O_2 \rightleftharpoons CO_2. \tag{9}$$

The following Pre-Exponential Adjustment (PEA) technique is used to obtain the correct flame speed for rich conditions by adjusting the forward reaction rates for the two reactions ($k_{f,1}$,$k_{f,2}$) at rich equivalence ratios [40]:

$$k_{f,1} = A_{r,1} f_1(\phi) e^{(-E_{a,1}/RT)} \left[C_3H_8\right]^{n_{C_3H_8}} \left[O_2\right]^{n_{O_2,1}} \tag{10}$$

$$k_{f,2} = A_{r,2} f_2(\phi) e^{(-E_{a,2}/RT)} \left[CO\right]^{n_{CO}} \left[O_2\right]^{n_{O_2,2}} \tag{11}$$

where the correction functions used are given by

$$f_1 = \frac{2}{\left[1 + \tanh\left(\frac{\phi_{0,1}-\phi}{\sigma_{0,1}}\right)\right] + b_1\left[1 + \tanh\left(\frac{\phi-\phi_{1,1}}{\sigma_{1,1}}\right)\right] + c_1\left[1 + \tanh\left(\frac{\phi-\phi_{2,1}}{\sigma_{2,1}}\right)\right]} \tag{12}$$

Table 1. Arrhenius kinetic constants: A_r is the pre-exponential factor and E_a is the activation energy. n_k is the reaction exponent relative to the species k.

	$A_r\ [cm^3/mol \cdot s]$	$E_a\ [cal/mol]$
$C_3H_8\ oxidation$	2.534×10^{11}	3.27×10^4
$n_{C_3H_8} = 0.845,$		
$n_{O_2,1} = 0.631$		
$CO - CO_2\ equilibrium$	2.0×10^9	1.2×10^4
$n_{CO} = 1.0,$		
$n_{O_2,2} = 0.5$		

$$f_2 = \frac{1}{2}\left[1+\tanh\left(\frac{\phi_{0,2}-\phi}{\sigma_{0,2}}\right)\right] + \frac{b_2}{2}\left[1+\tanh\left(\frac{\phi-\phi_{1,2}}{\sigma_{1,2}}\right)\right] + \\ + \frac{c_2}{2}\left[1+\tanh\left(\frac{\phi-\phi_{2,2}}{\sigma_{2,2}}\right)\right]\left[1+\tanh\left(\frac{\phi_{3,2}-\phi}{\sigma_{3,2}}\right)\right] \quad (13)$$

The Arrhenius kinetic constants, i.e., the pre-exponential factor A_r and the activation energy E_a are summarized in Tab. 1 while the coefficients used in the PEA functions are reported in Tab. 2. These values have been optimized to correctly retrieve the laminar flame speed (s_l^0) and thermal thickness (δ_l^0) of one-dimensional unstrained premixed flame propagating in fresh gases at different conditions ranging from $(340$ K, 3 bar$)$ to $(600$ K, 20 bar$)$. Pressure and temperature of fresh gases have been linked by an isentropic relation, as expected in an adiabatic chamber. A validation of the proposed mechanism in the CV2 operating conditions is shown in Fig. 6 where predictions of flame speed and thickness are compared with the ones obtained using the detailed mechanism from the CRECK modeling group [35].

The spark ignition is simulated using the ED model of Lacaze *et al.* [41]. Other works [14, 21, 25, 42] have revealed as the ED model is compatible with the TFLES. This model mimics the thermal effects of the spark discharge, adding, from a mathematical point of view, a source term to the energy equation. The LES solver computes the initial kernel development, even though

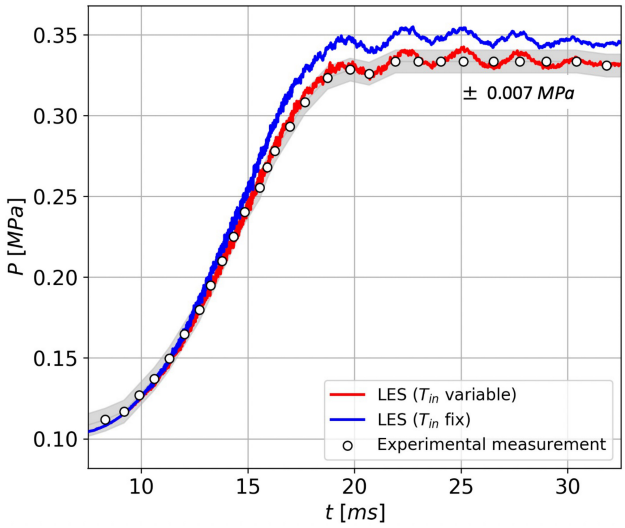

Fig. 8. Pressure signal (sensor in Fig. 1). Comparison between LES and experimental results ($\pm\ 0.007\ MPa$ of uncertainty). Computations have been done using the BC of the sect. 2 and compared with a simulation performed imposing a constant temperature ($T\ = 300\ K$) at the inlet.

Table 2. PEA coefficients of the correction functions used to correct the forward reaction rates.

	$\phi_{0,j}$	$\sigma_{0,j}$	b_j	$\phi_{1,j}$	$\sigma_{1,j}$	c_j	$\phi_{2,j}$	$\sigma_{2,j}$	$\phi_{3,j}$	$\sigma_{3,j}$
$j=1$	1.180	0.039	0.25	1.2	0.02	27.8	1.64	0.14	–	–
$j=2$	1.146	0.046	0.00015	1.2	0.04	0.025	1.215	0.03	1.32	0.09

the model is not able to represent all the plasma phases. Aside form the physical simplifications involved during the kernel formation, the ED model is able to reproduce the ignition dependence on mixing, predicting ignition failure due to mixture composition. Following the work of Pouech *et al.* [28], the energy deposition has been modeled using a Gaussian shape in space and rectangular in time between t_{start} and t_{end}. The shape of the spark corresponds to a cylinder of radius R_d and length L_{cyl}. Using cylindrical coordinates, the volumetric source term $\dot{Q}(r,z,t)$ can be expressed as follows:

$$\dot{Q}(r,z,t) = \frac{\epsilon_d}{2\pi a \sigma_t \sigma_s^2 L_{cyl}} exp\left(-\frac{1}{2}\frac{r^2}{\sigma_s^2}\right) \tag{14}$$

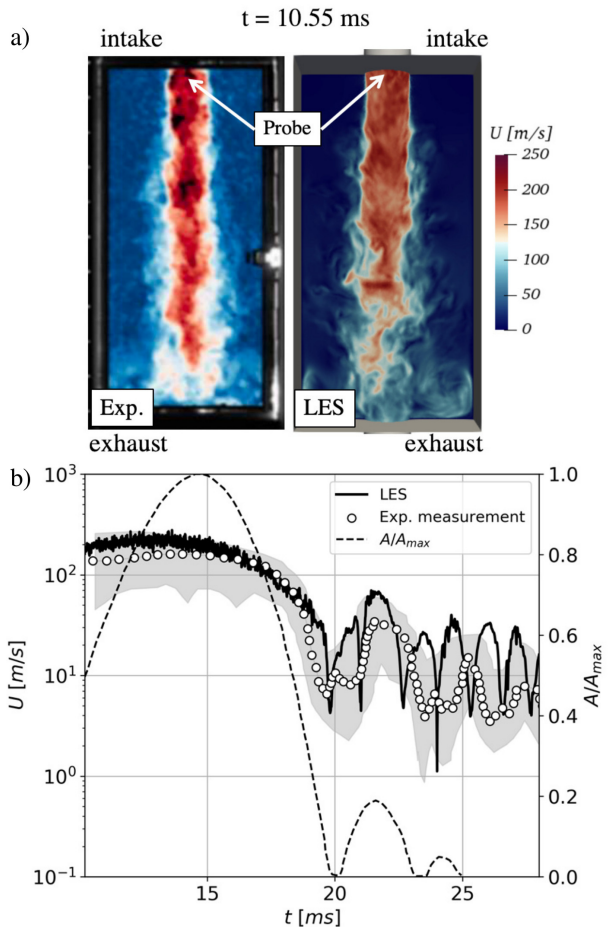

Fig. 9. a) Jet flow inside the central volume: comparison between LES simulation (top) and PIV measurements (bottom) at $t = 10.55\ ms$. Fuel is injected along the $z-$axis. b) Velocity magnitude measured at the intake: air inlet section, LES velocity magnitude, experimental velocity magnitude (averaged over all the experimental cycles).

where the energy ϵ_d corresponds to the $10 - 30\%$ of the total energy of an electric spark [43]. In this way, the losses due to thermal conduction to the electrodes, radiation, and shock wave expansion are taken into account (Tab. 3). In Eqn. (14), r is the distance to the center of the spark, σ_s and σ_t are parameters depending on the deposition size and its duration and defined as

$$\sigma_s = \frac{\Delta_s}{a}, \sigma_t = \frac{\Delta_t}{a} \tag{15}$$

where Δ_s is two times the spark radius R_d and Δ_t is $t_{end} - t_{start}$. This last parameter is chosen considering typical values found in literature [14, 28, 41] because it should be closer to the time in

Table 3. Parameters of the experimental and numerical spark.

	$Energy$ [mJ]	Δ_t [ms]	Δ_s [mm]
Experimental spark	40	2.5	3
Simulation spark	4	0.3	3

which heat is transferred to the fluid. The constant a ($a = 2\sqrt{\ln(10^{3.4})}$) is such that the 98% of the total energy ϵ_d is released inside the deposition volume $\Delta_s^3 \times \Delta_t$ [41]. In other words, the constant allows to verify that:

$$\int_{\Delta_s^3}\int_{\Delta_t} \dot{Q} dt dV = 0.98 \int_{-\infty}^{+\infty}\int_{-\infty}^{+\infty} \dot{Q} dt dV. \tag{16}$$

L_{cyl} is the cylindrical spark length ($L_{cyl} = 3$ mm). The spark parameters used in the simulation are summarized in Tab. 3 and compared with experimental data.

Once ignited, the flame is resolved on the LES grid using the DTFLES model. Differently from what proposed by Legier *et at.* [31] the model is adapted to work correctly in variable fresh gases conditions. Indeed, when the pressure and temperature of gases inside the chamber increase, the laminar flame thickness reduces (Fig. 6) and the thickening factor should be recomputed in order to guarantee a constant resolved flame thickness ($n\Delta x$ with n the desired number of points inside the flame front). The fresh gas thermodynamic state is computed assuming that it evolves following an isentropic law and the equivalence ratio is evaluated at each node of the domain. The interaction between flame and turbulence is modeled using the Charlette efficiency model [44]. The constant β ($\beta = 0.75$) is higher than the standard values as found for the efficiency models used in CVC cases [45] .

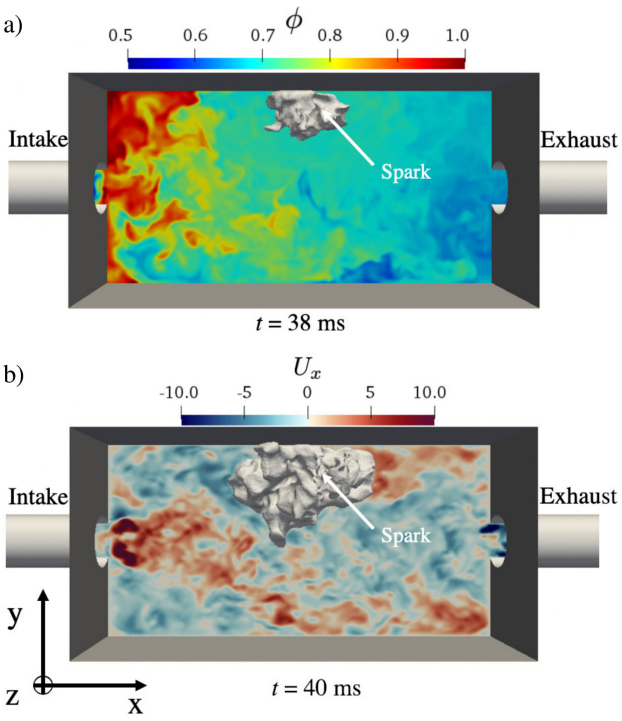

Fig. 10. Isosurfaces of temperature ($T = 1700\ K$) superimosed to the a) equivalence ratio field and b) x-velocity field.

RESULTS AND DISCUSSION

Admission phase

The admission phase starts with the air intake valve opening and ends at $t = 25.5$ ms when all the valves are closed. Propane is injected between $t = 9.5$ ms and $t = 18.7$ ms, when the air passage section reaches its maximum value (Fig. 2 (b)).

The correct mass flow rates of air and fuel are injected using the valve laws of Fig. 2 (b) at the air and fuel inlet boundary. This ensures the injection of the correct masses of air and fuel ($m_a \approx 633$ mg and $m_f \approx 39.5$ mg). In addition, the temperature at which the mass is injected (T_{in}) also varies in time: both air and fuel enter the chamber at a temperature lower than T^0 (Fig. 7 reports inlet temperature evolution for the air injection), because of their high speed (see Eqn. 5 or 6). This has a non-negligible impact on the chamber pressure: in Fig. 8, the pressure evolution recorded by a pressure transducer located inside the combustion chamber during the intake phase is compared with pressure evolutions predicted by two LES realizations of the intake process where a variable and constant inlet temperature is assumed. The correct pressure level

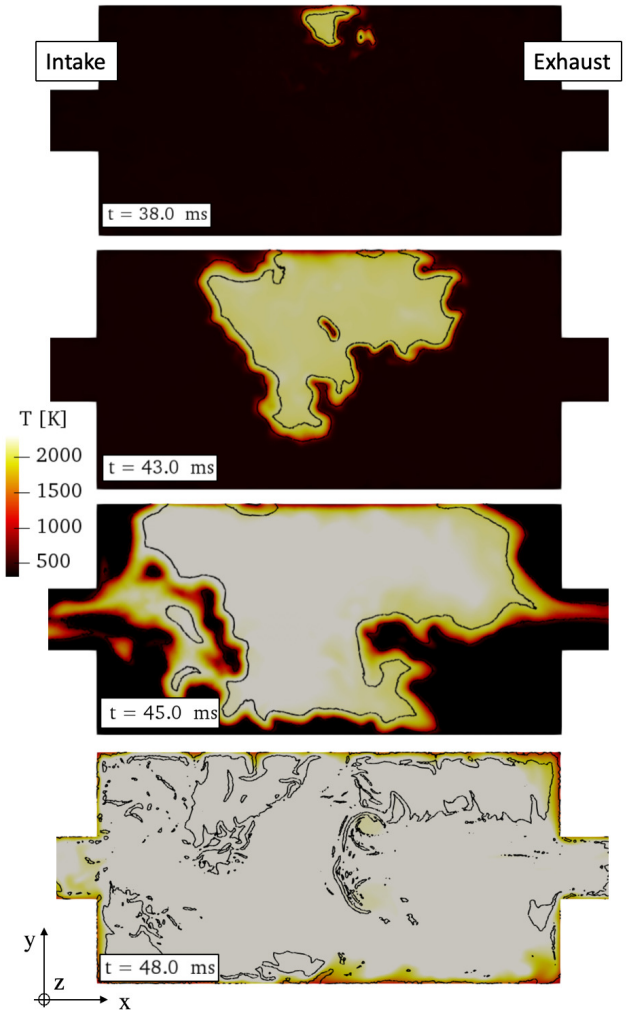

Fig. 11. Flame propagation inside the CVC. Isoline of heat release rate (10^8 - black solid line) superimposed on the temperature field in the ignition plane.

inside the chamber at the beginning of the combustion phase is only reached when the BC of Sect. 2 miming the valve law is considered.

Further validation of the simulations are proposed in Fig. 9 (a) where the velocity magnitude field predicted by the LES is compared with the PIV measurements at $t = 10.55$ ms. The shape and extension of the air jet flow entering the combustion chamber are in good agreement with experiments. A more quantitative comparison is performed in Fig. 9 (b) where the instantaneous velocity magnitude captured in the LES by a probe located as in the experiments (Fig. 9 (a)) matches the experimental trend of the averaged velocity on multiple cycles.

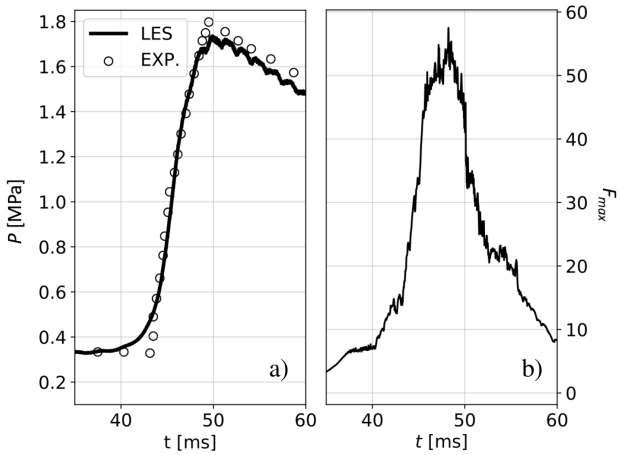

Fig. 12. a) Pressure signal (sensor in Fig. 1). Comparison between LES and experiments. b) Maximum thickening factor computed during the simulation.

Combustion phase

Ignition occurs in the longitudinal plane of the chamber (Fig. 1) and the flame propagates in the non-homogeneous mixture towards the richer region closer to the intake tube (Fig. 10 (a)): the kernel (Fig. 10 - isocontour of temperature) moves preferentially towards the intake, surrounded by turbulence activity (Fig. 10 (b)). The flame evolution is shown in Fig. 11 (isoline of heat release rate): after ignition ($t = 38$ ms) the flame propagates in the chamber and enters the two inlet/outlet pipes ($t = 43 - 45$ ms) until it finds enough fuel to burn . At $t = 48$ ms the totality of the available mixture has been consumed and the flame progressively loses its power.

Figure 12 (a) reports pressure evolution in the chamber compared with experimental recordings. As combustion evolves, pressure raises and the experimental peak at $t \approx 48$ ms is captured by the LES. Following the techniques explained in section 2, the maximum thickening factor increases (Fig. 12 (b)) as the flame gets thinner (Fig. 6). Then it decreases following the pressure behavior. The flow reaches approximately 1.8 MPa before the flame starts quenching on the inner walls of the chamber. During the entire cycle, walls are cold ($T_w \sim 307$ K [16]) and the burnt mixture undergoes an isochoric expansion: both pressure and temperature reduce in time while all the valves are still closed.

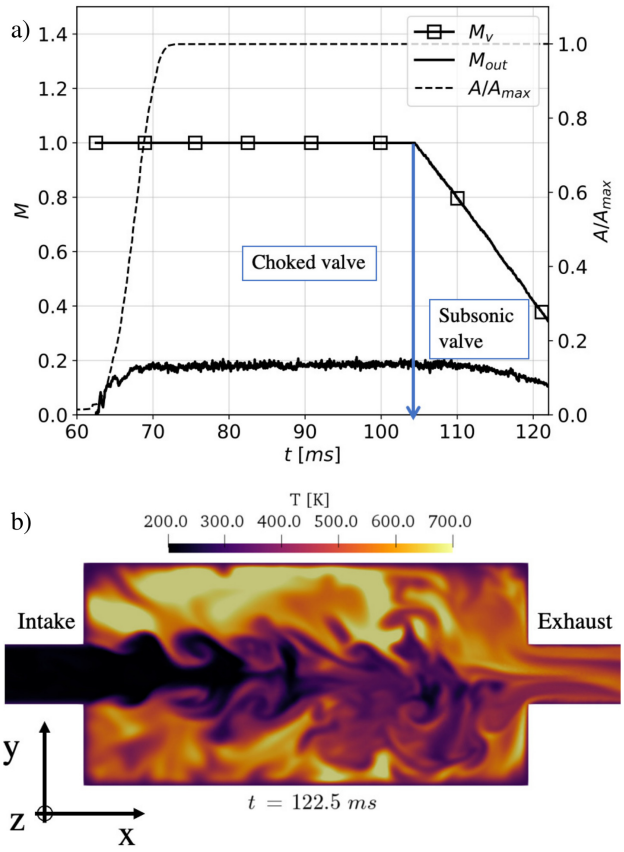

Fig. 13. a) Mach number M_v in the valve section and on the outlet computational domain, M_{out}. The dashed line represents the valve section law. b) Instantaneous temperature field at the end of the exhaust phase. Ignition plane (x-y).

Exhaust phase

At $t = 62.5$ ms the exhaust valve starts opening and connects the chamber with a tank at $P_{exh} = 1$ bar. Starting from 14 bar, the flow expands to the critical value P^* in the minimum section of the valve and then adapts to the exhaust conditions through non-isentropic processes. Here the fluid dynamic losses are taken into account with a $C_{d,exh} = 0.7$.

Figure 13 (a) reports the evolution of the Mach number M_v predicted in the valve section by the outlet BC and the corresponding M_{out} at the outlet of the computational domain. It is noted that the flow in the valve is sonic until $t = 104$ ms. Indeed, when the valve opens, the pressure in the chamber is such that the flow cannot expand to pressure values lower than the critical one. Therefore, the critical section $A_v = A^*$ decouples the outlet section of the domain (upstream the convergent of Fig. 5) from what happens downstream. When the choking condition is no longer

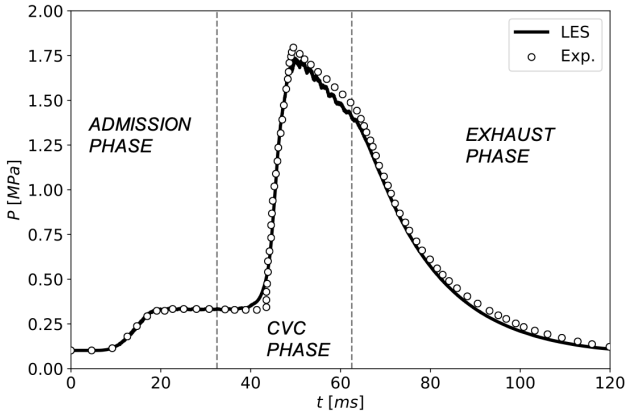

Fig. 14. Pressure signal (sensor in Fig. 1): complete reactive cycle. Comparison between LES simulation (solid line) and experimental results (dots).

verified, the mach number in the section of the valve starts reducing according to the following law:

$$M_v = \sqrt{\frac{2}{\gamma - 1}\left(\left(\frac{P_{out}^{0,LES}}{P_v}\right)^{\frac{\gamma-1}{\gamma}} - 1\right)}. \tag{17}$$

The stagnation pressure in the chamber tends to balance the exhaust pressure and the mass flow rate gets close to zero. During this phase, the flow is highly stratified because part of the cold mixture has been pushed at the ends of the pipes and compressed during the combustion phase. This leads to density differences which generate vortices when the pressure gradient drives the flow from the intake tube to the exhaust line as shown in Fig. 13 (b).

Finally, Fig. 14 shows the complete pressure signal recorded with a numerical probe placed in the same location as the pressure sensor in the experiments. A very good agreement is observed between the two signals for the three phases.

CONCLUSIONS

The Constant-Volume Combustion chamber, CV2, installed at the Pprime laboratory was numerically investigated using Large Eddy Simulation. The chamber is characterized by two high-speed solenoid valves controlling the intake and the exhaust. Concerning these two phases a

new modelling strategy was proposed: no moving body is introduced in the computational domain and the effect of the valves on the flow entering and leaving the chamber is included inside the boundary conditions to save computational cost. Relying on the shape of the path that the flow runs across the valves, the nozzles theory was used. The valve law as well as the tanks stagnation quantities are enough to impose the correct variables for both inlet and outlet. To model the combustion phase, a novel 2-steps chemistry was proposed and optimized to obtain the good laminar flame behavior for multiple fresh gases pressures and temperatures. The DTFLES model has been adapted to take into account pressure and temperature effects on the laminar flame thickness and speed. The ignition phase was simulated using the Energy Deposition model with a cylindrical shape to mimic the experimental spark. LES simulations are shown to be in good agreement with the experiments in terms of pressure signals and flow field. Comparison with PIV measurements showed that the flow activity was also well captured. The proposed modelling is therefore proved to be able to successfully predict the complex fluid and flame dynamics happening in such CVC system. Cycle-to-cycle variations will be the subject of future investigations.

ACKNOWLEDGEMENTS

This project has received funding from the European Union's Horizon 2020 research and innovation program under Grant Agreement No 956803 (INSPIRE - INSpiring Pressure gain combustion Integration, Research, and Education). This work was performed using HPC resources from GENCI-TGCC (Grant 2021- A0092B10157)

REFERENCES

[1] European Climate Foundation, 2020, Roadmap 2050 Tech. rep.

[2] Stathopoulos, P., 2018, "Comprehensive thermodynamic analysis of the humphrey cycle for gas turbines with pressure gain combustion," *Energies,* **11**(12).

[3] Heiser, W. H., and Pratt, D. T., 2002, "Thermodynamic cycle analysis of pulse detonation engines," *Journal of Propulsion and Power,* **18**(1), pp. 68–76.

[4] Jones, S. M., and Paxson, D. E., 2013, "Potential benefits to commercial propulsion systems

from pressure gain combustion," In *49th AIAA/ASME/SAE/ASEE Joint Propulsion Conference*, Vol. 1 PartF. American Institute of Aeronautics and Astronautics Inc.

[5] Kailasanath, K., 2020, *Recent Developments in the Research on Pressure-Gain Combustion Devices* Springer Singapore.

[6] Bluemner, R., Bohon, M. D., Paschereit, C. O., and Gutmark, E. J., 2019, "Experimental Study of Reactant Mixing in Model Rotating Detonation Combustor Geometries," *Flow, Turbulence and Combustion,* **102**(2), pp. 255–277.

[7] Duvall, J., Chacon, F., Harvey, C., and Gamba, M., 2018, "Study of the effects of various injection geomteries on the operation of a rotating detonation engine," In *AIAA Aerospace Sciences Meeting, 2018*, no. 210059. American Institute of Aeronautics and Astronautics Inc, AIAA.

[8] Gray, J. A., Lemke, M., Reiss, J., Paschereit, C. O., Sesterhenn, J., and Moeck, J. P., 2017, "A compact shock-focusing geometry for detonation initiation: Experiments and adjoint-based variational data assimilation," *Combustion and Flame,* **183**, pp. 144–156.

[9] Wolański, P., 2013, "Detonative propulsion," *Proceedings of the Combustion Institute,* **34**(1), pp. 125–158.

[10] Bobusch, B. C., Berndt, P., Paschereit, C. O., and Klein, R., 2014, "Shockless explosion combustion: An innovative way of efficient constant volume combustion in gas turbines," *Combustion Science and Technology,* **186**(10-11), pp. 1680–1689.

[11] Hutchins, T. E., and Metghalchi, M., 2003, "Energy and exergy analyses of the pulse detonation engine," *Journal of Engineering for Gas Turbines and Power,* **125**(4), pp. 1075–1080.

[12] Yücel, F. C., Habicht, F., Bohon, M. D., and Paschereit, C. O., 2021, "Autoignition in stratified mixtures for pressure gain combustion," *Proceedings of the Combustion Institute,* **38**(3), pp. 3815–3823.

[13] Boust, B., Michalski, Q., and Bellenoue, M., 2016, "Experimental investigation of ignition and combustion processes in a constant-volume combustion chamber for air-breathing propulsion," In *52nd AIAA/SAE/ASEE Joint Propulsion Conference, 2016*. pp. 1–8.

[14] Labarrere, L., Poinsot, T., Dauptain, A., Duchaine, F., Bellenoue, M., and Boust, B., 2016,

"Experimental and numerical study of cyclic variations in a Constant Volume Combustion chamber," *Combustion and Flame,* **172**, pp. 49–61.

[15] Michalski, Q., Boust, B., and Bellenoue, M., 2019, "Influence of operating conditions and residual burned gas properties on cyclic operation of constant-volume combustion," In *Notes on Numerical Fluid Mechanics and Multidisciplinary Design*, R. King, ed., Vol. 141. Springer International Publishing, pp. 215–233.

[16] Michalski, Q., 2019, "Étude expérimentale de la combustion à volume constant pour la propulsion aérobie : influence de l'aérodynamique et de la dilution sur l'allumage et la combustion," PhD thesis, École Nationale Superieure De Mecanique et d'Aerotechnique.

[17] Michalski, Q., Boust, B., and Bellenoue, M., 2018, "Toward a cyclic self-ignited constant-volume combustion for airbreathing propulsion applications," In 2018 Joint Propulsion Conference.

[18] Michalski, Q., Kha, K. Q., Robin, V., Boust, B., Mura, A., and Bellenoue, M., 2018, "Joint numerical and experimental characterization of the turbulent reactive flow within a constant volume vessel," In 2018 Joint Propulsion Conference, pp. 1–12.

[19] Michalski, Q., Boust, B., and Bellenoue, M., 2019, "Experimental Investigation of Ignition Stability in a Cyclic Constant-Volume Combustion Chamber Featuring Relevant Conditions for Air-Breathing Propulsion," *Flow, Turbulence and Combustion,* **102**(2), pp. 279–298.

[20] Tagliante, F., Poinsot, T., Pickett, L. M., Pepiot, P., Malbec, L. M., Bruneaux, G., and Angelberger, C., 2019, "A conceptual model of the flame stabilization mechanisms for a lifted Diesel-type flame based on direct numerical simulation and experiments," *Combustion and Flame,* **201**, pp. 65–77.

[21] Enaux, B., Granet, V., Vermorel, O., Lacour, C., Pera, C., Angelberger, C., and Poinsot, T., 2011, "LES study of cycle-to-cycle variations in a spark ignition engine," *Proceedings of the Combustion Institute,* **33**(2), pp. 3115–3122.

[22] Xu, G., Kotzagianni, M., Kyrtatos, P., Wright, Y. M., and Boulouchos, K., 2019, "Experimental and numerical investigations of the unscavenged prechamber combustion in a rapid compression and expansion machine under engine-like conditions," *Combustion and Flame,* **204**,

pp. 68–84.

[23] Hasse, C., Sohm, V., and Durst, B., 2010, "Numerical investigation of cyclic variations in gasoline engines using a hybrid URANS/LES modeling approach," *Computers and Fluids,* **39**(1), pp. 25–48.

[24] Vermorel, O., Richard, S., Colin, O., Angelberger, C., Benkenida, A., and Veynante, D., 2009, "Towards the understanding of cyclic variability in a spark ignited engine using multi-cycle LES," *Combustion and Flame,* **156**, pp. 1525–1541.

[25] Granet, V., Vermorel, O., Lacour, C., Enaux, B., Dugué, V., and Poinsot, T., 2012, "Large-Eddy Simulation and experimental study of cycle-to-cycle variations of stable and unstable operating points in a spark ignition engine," *Combustion and Flame,* **159**, pp. 1562–1575.

[26] Malé, Q., Staffelbach, G., Vermorel, O., Misdariis, A., Ravet, F., and Poinsot, T., 2019, "Large Eddy Simulation of Pre-Chamber Ignition in an Internal Combustion Engine," *Flow, Turbulence and Combustion,* **103**(2), pp. 465–483.

[27] Misdariis, A., Vermorel, O., and Poinsot, T., 2015, "A methodology based on reduced schemes to compute autoignition and propagation in internal combustion engines," *Proceedings of the Combustion Institute,* **35**(3), pp. 3001–3008.

[28] Pouech, P., Duchaine, F., and Poinsot, T., 2021, "Premixed flame ignition in high-speed flows over a backward facing step," *Combustion and Flame,* **229**.

[29] Poinsot, T., 2017, "Prediction and control of combustion instabilities in real engines," *Proceedings of the Combustion Institute,* **36**(1), pp. 1–28.

[30] Kazmouz, S. J., Haworth, D. C., Lillo, P., and Sick, V., 2021, "Large-eddy simulations of a stratified-charge direct-injection spark-ignition engine: Comparison with experiment and analysis of cycle-to-cycle variations," *Proceedings of the Combustion Institute,* **38**(4), pp. 5665–5672.

[31] Legier, J. P., Poinsot, T., and Veynante, D., 2000, "Dynamically thickened flame LES model for premixed and non-premixed turbulent combustion," *Proceedings of the Summer Program, Centre for Turbulence Research*.

[32] Colin, O., and Rudgyard, M., 2000, "Development of High-Order Taylor-Galerkin Schemes for

LES," *Journal of Computational Physics,* **162**(2), pp. 338–371.

[33] Colin, O., Benkenida, A., and Angelberger, C., 2003, "3D modeling of mixing, ignition and combustion phenomena in highly stratified gasoline engines," *Oil and Gas Science and Technology,* **58**(1), pp. 47–62.

[34] Nicoud, F., and Ducros, F., 1999, "Subgrid-scale stress modelling based on the square of the velocity gradient tensor," *Flow, Turbulence and Combustion,* **62**(3), pp. 183–200.

[35] Ranzi, E., Frassoldati, A., Stagni, A., Pelucchi, M., Cuoci, A., and Faravelli, T., 2014, "Reduced kinetic schemes of complex reaction systems: Fossil and biomass-derived transportation fuels," *International Journal of Chemical Kinetics,* **46**(9), pp. 512–542.

[36] Poinsot, T. J., and Lelef, S. K., 1992, "Boundary conditions for direct simulations of compressible viscous flows," *Journal of Computational Physics,* **101**(1), pp. 104–129.

[37] Shapiro, A. H., 1954, *The Dynamics and thermodynamics of compressible fluid flow / by Ascher H. Shapiro*, Vol. II.

[38] Beavis, N. J., Ibrahim, S. S., and Malalasekera, W., 2018, "Numerical Evaluation of Combustion Regimes in a GDI Engine," *Flow, Turbulence and Combustion,* **101**(4), pp. 1035–1057.

[39] Jamil, A., Baharom, M. B., and A. Aziz, A. R., 2021, "IC engine in-cylinder cold-flow analysis – A critical review," *Alexandria Engineering Journal,* **60**(3), pp. 2921–2945.

[40] Franzelli, B., Riber, E., Sanjosé, M., and Poinsot, T., 2010, "A two-step chemical scheme for kerosene-air premixed flames," *Combustion and Flame,* **157**, pp. 1364–1373.

[41] Lacaze, G., Richardson, E., and Poinsot, T., 2009, "Large eddy simulation of spark ignition in a turbulent methane jet," *Combustion and Flame,* **156**, pp. 1993–2009.

[42] Zembi, J., Battistoni, M., Nambully, S. K., Pandal, A., Mehl, C., and Colin, O., 2021, "LES investigation of cycle-to-cycle variation in a SI optical access engine using TFM-AMR combustion model," *International Journal of Engine Research*.

[43] Maly, R., and Vogel, M., 1979, "Initiation and propagation of flame fronts in lean CH4-air mixtures by the three modes of the ignition spark," *Symposium (International) on Combustion,* **17**(1), pp. 821–831.

[44] Charlette, F., Meneveau, C., and Veynante, D., 2002, "A power-law flame wrinkling model

for LES of premixed turbulent combustion Part I: Non-dynamic formulation and initial tests," *Combustion and Flame,* **131**, pp. 159–180.

[45] Labarrere, L., 2016, "Étude théorique et numérique de la combustion à volume constant appliquée à la propulsion," PhD thesis, Institut National Polytechnique de Toulouse (INP Toulouse).

LIST OF FIGURES

LIST OF TABLES